Crystal Structure of 4,6-α-Glucanotransferase Supports Diet-Driven Evolution of GH70 Enzymes from α-Amylases in Oral Bacteria

Bai, Yuxiang; Gangoiti , Joana; Dijkstra, Bauke W; Dijkhuizen, Lubbert; Pijning, Tjaard

Published in:
Structure

DOI:
10.1016/j.str.2016.11.023

Document Version
Publisher's PDF, also known as Version of record

Publication date:
2017

Article

Structure

Crystal Structure of 4,6-α-Glucanotransferase Supports Diet-Driven Evolution of GH70 Enzymes from α-Amylases in Oral Bacteria

Graphical Abstract

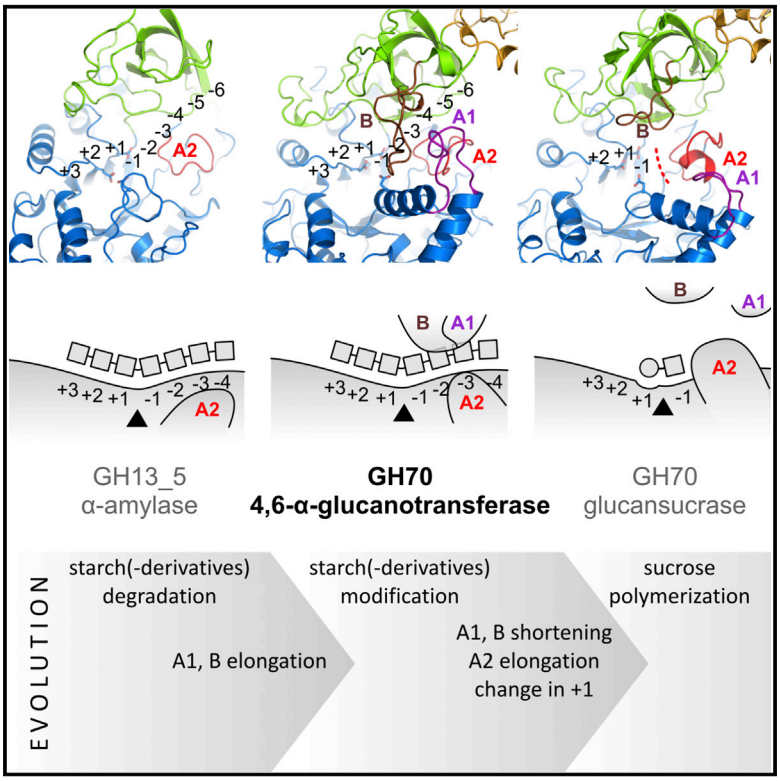

Authors

Yuxiang Bai, Joana Gangoiti, Bauke W. Dijkstra, Lubbert Dijkhuizen, Tjaard Pijning

Correspondence

t.pijning@rug.nl

In Brief

Bai et al. present the first crystal structure of a 4,6-α-glucanotransferase, explaining their mode of action and detailing the structural changes accompanying the proposed evolution of glycoside hydrolase family 70 (GH70) glucansucrases from starch-acting GH13 amylases in oral bacteria, supported by genomic and phylogenetic studies.

Highlights

- *L. reuteri* 121 GtfB-ΔNΔV structure explains 4,6-α-glucanotransferase mode of action
- Suggests loop changes accompanied evolution of glucansucrases from α-amylases
- Genomic, phylogenetic, and in vivo studies support such an evolutionary pathway
- Dietary carbohydrate changes may have triggered the relevant evolutionary events

Bai et al., 2017, Structure *25*, 231–242
February 7, 2017
http://dx.doi.org/10.1016/j.str.2016.11.023

Structure
Article

Crystal Structure of 4,6-α-Glucanotransferase Supports Diet-Driven Evolution of GH70 Enzymes from α-Amylases in Oral Bacteria

Yuxiang Bai,[1,3] Joana Gangoiti,[1] Bauke W. Dijkstra,[2] Lubbert Dijkhuizen,[1] and Tjaard Pijning[2,4,*]
[1]Laboratory of Microbial Physiology
[2]Laboratory of Biophysical Chemistry
Groningen Biomolecular Sciences and Biotechnology Institute (GBB), University of Groningen, Nijenborgh 7, 9747 AG Groningen, the Netherlands
[3]Present address: The State Key Laboratory of Food Science and Technology, School of Food Science and Technology, Jiangnan University, Wuxi 214122, China
[4]Lead Contact
*Correspondence: t.pijning@rug.nl
http://dx.doi.org/10.1016/j.str.2016.11.023

SUMMARY

Food processing and refining has dramatically changed the human diet, but little is known about whether this affected the evolution of enzymes in human microbiota. We present evidence that glycoside hydrolase family 70 (GH70) glucansucrases from lactobacilli, synthesizing α-glucan-type extracellular polysaccharides from sucrose, likely evolved from GH13 starch-acting α-amylases, via GH70 4,6-α-glucanotransferases. The crystal structure of a 4,6-α-glucanotransferase explains the mode of action and unique product specificity of these enzymes. While the α-amylase substrate-binding scaffold is retained, active-site loops adapted to favor transglycosylation over hydrolysis; the structure also gives clues as to how 4,6-α-glucanotransferases may have evolved further toward sucrose utilization instead of starch. Further supported by genomic, phylogenetic, and in vivo studies, we propose that dietary changes involving starch (and starch derivatives) and sucrose intake were critical factors during the evolution of 4,6-α-GTs and glucansucrases from α-amylases, allowing oral bacteria to produce extracellular polymers that contribute to biofilm formation from different substrates.

INTRODUCTION

Lactobacillus and *Streptococcus* are key plaque-forming oral bacteria that ferment dietary carbohydrates in the oral cavity, thereby producing acids that dissolve calcium phosphate in the tooth enamel. They synthesize long-chain, branched polymers containing repeating units of sugars or sugar derivatives. These extracellular polysaccharides (EPS) are largely undegradable by α-amylases (Carlsson et al., 1975; Leemhuis et al., 2013b), and form a protective layer around the bacteria and facilitate biofilm formation, promoting adhesion of the bacteria to the tooth enamel (Flemming and Wingender, 2010; Koo et al., 2010; Xiao et al., 2012). The EPS are thus an important causative factor for the development of dental caries (Koo et al., 2013) and, as a consequence, the presence of sucrose in many kinds of food contributes to a worldwide health problem (Paes Leme et al., 2006). However, sucrose is only a rather recent addition to the human diet, with starch from staple foods still being the major source of carbohydrates (Yudkin, 1967). This raises the question of whether oral bacteria also use starch or starch-derived oligosaccharides instead of sucrose for polysaccharide production.

The sucrose-derived EPS are synthesized by glucansucrases (GSs) (Leemhuis et al., 2013a) that are classified in glycoside hydrolase family 70 (GH70; www.cazy.org; Lombard et al., 2014), but share sequence homology with α-amylases of GH13, which mainly hydrolyze starch and starch-derived oligosaccharides. The core domains of GSs and α-amylases have similar folds, but the GSs have a circularly permuted $(\beta/\alpha)_8$ barrel in the catalytic domain, and contain additional N- and C-terminal domains that are absent in α-amylases (Leemhuis et al., 2013a; Vujičić-Žagar et al., 2010). It has been proposed that this domain organization of GSs evolved from an ancestral α-amylase via gene duplication, truncation, and domain insertion events (Vujičić-Žagar et al., 2010). However, little is known about how GSs would have evolved from α-amylases to be able to synthesize EPS from sucrose.

Recently, several GH70 enzymes were identified in *Lactobacillus* species that, instead of acting on sucrose, utilize starch-derived oligosaccharides as substrates, and synthesize α-glucans with a high degree of α-1,6-linkages (Kralj et al., 2011; Dobruchowska et al., 2012; Leemhuis et al., 2014; Bai et al., 2015, 2016a). Thus, the activity of these 4,6-α-glucanotransferase enzymes (4,6-α-GTs) has characteristics of both α-amylases and GSs. The 4,6-α-GTs share 45%–50% sequence identity with GSs, but form a phylogenetically distinct GH70 subfamily with clear amino acid differences and distinctive insertions/deletions in some of the loops in the core domains (Kralj et al., 2011; Leemhuis et al., 2013a).

Table 1. Crystallographic Data

	Native (Wild-Type)	Maltohexaose Soak (Wild-Type)	Maltopentaose Soak (D1015N)
PDB entry	5JBD	5JBE	5JBF
Data Collection			
Space group	*C* 2	*C* 2	*C* 2
Cell dimensions *a*, *b*, *c* (Å)	219.2, 57.9, 150.7	220.4, 58.3, 151.4	219.5, 58.1, 150.4
β (°)	114.7	114.3	114.4
Resolution (Å)	136.8–1.80 (1.83–1.80)	138.1–2.10 (2.14–2.10)	138.0–2.19 (2.23–2.19)
R_{merge} (%)	0.080 (0.808)	0.126 (0.818)	0.061 (0.354)
$\langle I/\sigma \rangle$	10.2 (2.0)	7.7 (2.1)	8.2 (2.2)
Completeness (%)[a]	99.3 (97.1)	99.2 (98.9)	90.2 (90.5)
Redundancy[a]	4.3 (4.3)	4.0 (3.7)	2.2 (2.2)
Refinement			
Resolution (Å)	45.8–1.80 (1.83–1.80)	46.2–2.10 (2.14–2.10)	48.0–2.19 (2.23–2.19)
Unique observations[a]	15,308 (7,585)	102,167 (4,956)	80,800 (4,647)
R/R_{free}	0.187/0.216	0.208/0.239	0.199/0.242
No. of atoms			
Protein	13,415	13,356	13,356
Ca^{2+}/waters	2/1283	2/623	2/703
Carbohydrate ligands	–	6^4-α-D-glucosyl-maltotetraose (2), maltose (1), glucose (1)	maltopentaose (2), maltotriose (1), maltose (4)
Other ligand molecules	acetate (5), sulfate (4), glycerol (9), triethylene glycol (1)	acetate (6), sulfate (4)	sulfate (5)
B factors			
Protein ($Å^2$)	33.3	39.0	42.4
Carbohydrate ($Å^2$)	–	59.7 (6^4-α-D-glucosyl-maltotetraose), 55.7 (maltose)	42.3 (maltopentaose), 49.4 (maltotriose), 52.1 (maltose)
Rmsd			
Bond lengths (Å)	0.0086	0.0075	0.0075
Bond angles (°)	1.17	1.13	1.21
Ramachandran			
Favored (%)	97.7	97.5	96.6
Allowed (%)	2.0	2.3	3.2
Outliers (%)	0.2	0.1	0.2

[a]In highest shell: between brackets.

Here we provide biochemical, 3D structural, genomic, and phylogenetic data for a 4,6-α-glucanotransferase from *Lactobacillus reuteri* 121 (GtfB) that support a, probably diet-driven, evolution from a maltooligosaccharide-processing α-amylase to present-day GSs, via a 4,6-α-GT-like intermediate.

RESULTS

Overall Structure

The 1.80-Å resolution crystal structure (Table 1) of the core of the 4,6-α-glucanotransferase GtfB from *L. reuteri* 121 (GtfB-ΔNΔV, residues 762-1619-His_6) revealed that each of the two GtfB-ΔNΔV molecules in the asymmetric unit comprises the glucansucrase-like domains A, B, C, and IV (Figure 1A), with very similar structures to those of other GH70 enzymes (Vujičić-Žagar et al., 2010; Ito et al., 2011; Pijning et al., 2012; Brison et al., 2012). In dynamic light-scattering measurements, GtfB-ΔNΔV behaves as an ~85-kDa particle, showing that the enzyme is monomeric in solution (see Supplemental Experimental Procedures). The location of the N terminus, at the protein surface of GtfB-ΔNΔV and fully solvent accessible, suggests that the additional N-terminal domain can be accommodated without affecting the structure of the core of the protein. The polypeptide chain follows a "U-course" (Vujičić-Žagar et al., 2010), forming first the N-terminal halves of domains IV, B, and A, then the complete C domain, and finally the C-terminal halves of domains A, B, and IV (Figure 1A). Thus, as in other GH70 enzymes, the $(\beta/\alpha)_8$ barrel of the catalytic domain A is circularly permuted, and the order of the four conserved sequence motifs (II-III-IV-I) in the amino acid sequence differs from GH13 α-amylases. At the interface of the A and B domains, several residues that are strictly conserved in GH13 and GH70 enzymes surround a pocket that harbors subsites −1 and +1 of the active site (see below; subsite nomenclature according to Davies et al., 1997).

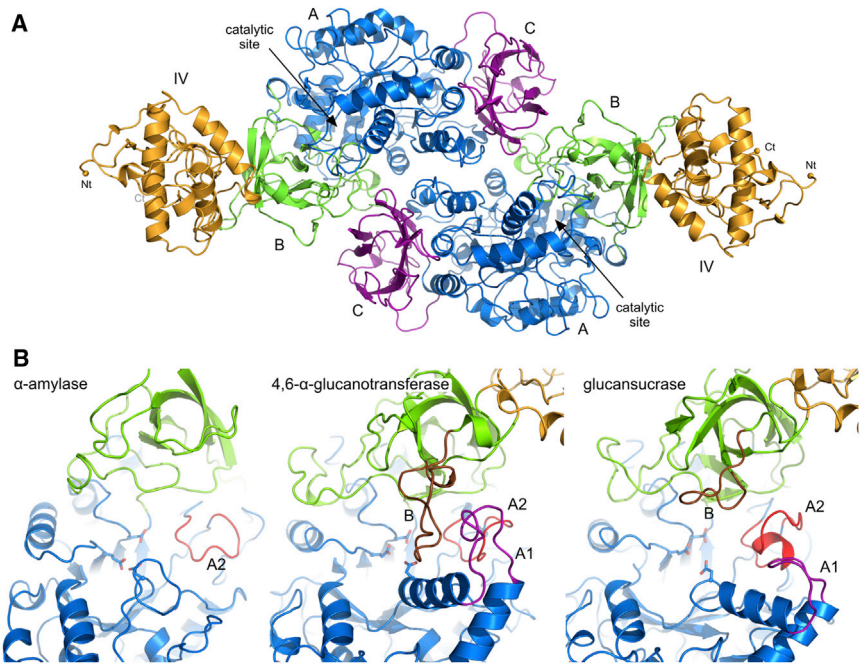

Figure 1. Crystal Structure of GtfB-ΔNΔV Compared with α-Amylases and Glucansucrases

(A) Crystal structure of GtfB-ΔNΔV showing the two molecules in the asymmetric unit. From the N-terminal residue (Nt) the polypeptide forms the N-terminal segments of domains IV (yellow), B (green), and A (blue), then domain C (purple) and the C-terminal segments of domains A, B, and IV toward the C-terminal residue (Ct).

(B) Arrangement of loops A1, A2, and B around the active site of GH13 α-amylases (left), 4,6-α-glucanotransferases (middle), and GH70 glucansucrases (right), at the interface of the catalytic domain A (blue) and domain B (green). Looking down the $(\beta/\alpha)_8$ barrel, acceptor subsites are on the left and donor subsites on the right; catalytic residues are shown as sticks. Structures used are *Bacillus licheniformis* α-amylase (PDB: 1BLI; Machius et al., 1998), GtfB-ΔNΔV (this work), and *Lactobacillus reuteri* 180 Gtf180-ΔN (PDB: 3KLK; Vujičić-Žagar et al., 2010).

Active-Site Architecture: Comparison with α-Amylases and Glucansucrases

GtfB-ΔNΔV shows structural similarity to both GH13 α-amylases and GH70 glucansucrases. Yet important differences are present in the arrangement of three loops near the active site (Figure 1B); sequence alignments of the regions containing these loops (Figure 2A) show that they are unique to 4,6-α-GTs and more conserved than within GSs.

Regarding GH13 α-amylases, the A + B domains of GtfB-ΔNΔV are most similar to the A + B domains of the α-amylase from *Bacillus licheniformis* (Machius et al., 1998) (root-mean-square deviation [rmsd] of 2.10 Å). At the interface between these domains, both enzymes have a long groove which makes a bend near the active-site pocket. Two loops in GtfB-ΔNΔV, which have no equivalent in α-amylases, fold over the donor side of the binding groove and create a tunnel-like structure (Figures 1B and 3). First, "loop A1" (residues 1,139–1,151) in the helix-loop-helix subdomain inserted between strand β4 and helix α5 forms a large protrusion toward domain B. Adjacent to loop A1, a long loop containing residues 905–924 ("loop B") folds over the groove from the opposite direction. A third loop, connecting strand β7 and helix α8 of the $(\beta/\alpha)8$ barrel ("loop A2," residues 1,430–1,440) lies below loops A1 and B.

The structurally closest glucansucrase homolog of GtfB-ΔNΔV is GTF180-ΔN from *L. reuteri* 180 (Vujičić-Žagar et al., 2010); their A + B domains can be superimposed with an rmsd of 0.84 Å. Notable differences exist at the donor subsites. The tunnel-forming loops A1 and B of GtfB-ΔNΔV are longer than their GTF180-ΔN counterparts and create a less open arrangement compared with GSs. Notably, loop A2 of GtfB-ΔNΔV at the base of the tunnel is shorter than the equivalent loop in GTF180-ΔN, lacks a short α helix, and does not block access to donor subsites beyond −1.

The catalytic subsite −1 of GtfB-ΔNΔV is very similar to that of α-amylases and GSs; six of the seven conserved GH13 residues are present (the three catalytic residues D1015, E1053, and D1125, as well as residues R1013, H1124, and D1479); the seventh residue, a histidine, is replaced by a glutamine (Q1484) as in GSs (Figure 4).

On the other hand, sequence alignment of motifs I, III, and IV (Figure 2B) shows that the 4,6-α-GTs form a highly conserved and separate group; regarding subsite +1, there are a few notable differences with GSs. For example, a tyrosine residue (Y1055 in motif III) replaces the tryptophan residue found in almost all glucansucrases; although it may provide an aromatic stacking interaction with glucosyl units as in GS structures (Vujičić-Žagar et al., 2010; Ito et al., 2011), it cannot provide a hydrogen bond to sugar units in subsite +1. Moreover, residue K1128 replaces the conserved glutamine residue of GSs in motif IV. The importance of these residues for enzyme activity and specificity is shown by site-directed mutagenesis experiments; mutation of Y1055 or K1128 greatly affected the ability of the enzyme to synthesize polymers, and/or its α-1,6 transglycosylation activity (Table S1; Figures S1 and S2, related to Figure 4A). Whereas wild-type GtfB 4,6-α-glucanotransferase activity results in the conversion of amylose to isomalto-/maltopolysaccharides with a relatively high percentage of α-1,6 linkages, Y1055G and K1128 mutants mainly displayed endo-α-1,4-glycosidase activity and hydrolyzed the amylose polymer to maltooligosaccharides. Finally, residues from domain B (e.g., L971, V972) cause one side of subsite +1 to be somewhat wider in GtfB-ΔNΔV (Figure 4A).

Interaction with Oligosaccharides

Soaking experiments with crystals of wild-type enzyme and the inactive D1015N mutant, and a range of glucooligosaccharides (degree of polymerization [DP] DP2–DP7) resulted in binding of oligosaccharides in the donor subsites (−1, −2, etc.), but never in the acceptor subsites (+1, +2 etc.). Maltopentaose (G5) binds in subsites −1 to −5 with its reducing end in

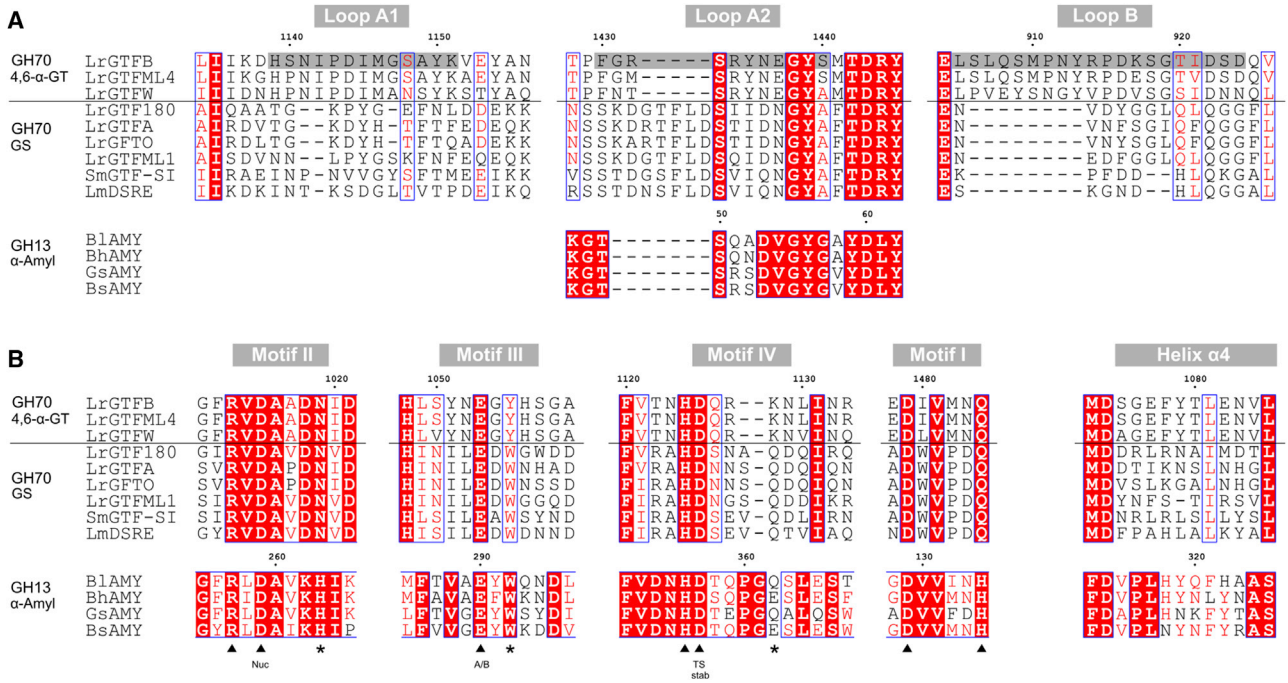

Figure 2. Sequence Alignment of 4,6-α-Glucanotransferase, Glucansucrases, and α-Amylases

Alignments were made using ESPript v3.0 (Robert and Gouet, 2014). Numbering corresponds to the sequences of LrGtfB and BlAMY.

(A) Loop regions around the active site: loops A1, A2 and B (gray shading); α-amylases (α-Amyl) were aligned only for loop A2 since these enzymes do not have an equivalent to loops A1 and B.

(B) Conserved motifs I–IV, and the region containing helix α4. The seven conserved α-amylase superfamily residues are indicated (arrowheads), including the catalytic residues (Nuc, nucleophile; A/B, general acid/base; TS stab, transition state stabilizing residue). Other residues near subsites −1 and +1 are indicated (asterisks).

4,6-α-Glucanotransferases (4,6-α-GT): LrGTFB, *L. reuteri* 121 GtfB; LrGTFML4, *L. reuteri* ML1 GtfML4; LrGTFW, *L. reuteri* DSM 20016 GtfW. Glucansucrases (GS): LrGTF180, *L. reuteri* 180 Gtf180; LrGTFA, *L. reuteri* 121 GtfA; LrGTFO, *L. reuteri* ATCC 55730 GtfO; LrGTFML1, *L. reuteri* ML1 GtfML1; SmGTF-SI, *Streptococcus mutans* Gtf-SI; LmDSRE, *Leuconostoc mesenteroides* NRRL B-1299 DSRE. α-Amylases: BlAMY, *Bacillus licheniformis* α-amylase; BhAMY, *Bacillus halmapalus* α-amylase; GsAMY, *Geobacillus stearothermophilus* α-amylase; BsAMY, *Bacillus subtilis* KSM-K38 α-amylase.

subsite −1 (Figures 3A, 3B, S3A, and S4A) in a similar way as in ligand-bound α-amylase structures (e.g., α-amylase from *B. licheniformis* [Machius et al., 1998]). Most of the ligand-protein interactions are observed in subsites −1, −2, and −3; in particular, the reducing end glucosyl unit bound in subsite −1 has numerous hydrogen-bonding interactions with the conserved GH13/GH70 residues. In other donor subsites, residues from loops A1 and A2 (subsites −2, −3) and from loops in domain B (subsites −4, −5) provide most of the direct or water-mediated hydrogen-bonding interactions to the bound substrate. Notably, loops A1 and B shield subsites −2 and −3 from the solvent.

In contrast, soaking of wild-type GtfB-ΔNΔV crystals with maltohexaose (G6) yielded a pentasaccharide bound in subsites −2 to −6 (Figures 3C, 3D, S3B, and S4B). Interestingly, the non-reducing end glucosyl unit of the oligosaccharide bound in subsite −6 is α-1,6-linked, probably arising from a transglycosylation event; it has a stacking interaction with Y1521, a residue which is conserved in all 4,6-α-GTs. In subsite −1, some positive electron density is visible, but not enough to convincingly model a complete glucosyl unit. These results show that the enzyme exhibits α-1,6-transferase activity under the soaking conditions.

To investigate donor substrate binding in positive subsites, we superimposed a G5 bound in subsites −3 to +2 of *B. subtilis* α-amylase (Fujimoto et al., 1998) on the G5 bound in GtfB-ΔNΔV. The glucosyl moiety in subsite −1 superimposed almost perfectly, while those in subsites +1 and +2 needed only minor adjustments of glycosidic torsion angles to avoid clashes in GtfB-ΔNΔV (Figure 5A). Thus, maltooligosaccharide donor substrates likely bind in GtfB-ΔNΔV in a similar way as in α-amylases. To model acceptor binding, we constructed a covalent glucosyl-enzyme intermediate based on the experimentally observed structure of a cyclodextrin glycosyltransferase covalent intermediate (Uitdehaag et al., 1999). Subsequent manual docking of panose (O-α-D-glucopyranosyl-(1,6)-O-α-D-glucopyranosyl-(1,4)-D-glucose) in subsites +1 to +3 resulted in a productive orientation, with the non-reducing end 6-OH group pointing toward the anomeric C1 atom of the covalently linked glucosyl intermediate (Figure 5B). Residues possibly interacting with panose include N1019, E1053 (the catalytic acid/base), Y1055, Y1079, and N1129. Superposition of the donor and acceptor binding models (Figure 5C) shows that, with respect to the "canonical" α-amylase-like donor mode, the non-reducing end glucosyl of an acceptor in subsite +1 is rotated and slightly shifted to favor α-1,6-transglycosylation. Residues likely interacting with this glucosyl unit, N1019 and E1053 (the catalytic acid/base), are fully conserved among characterized 4,6-α-GTs and GSs (Figure 2B).

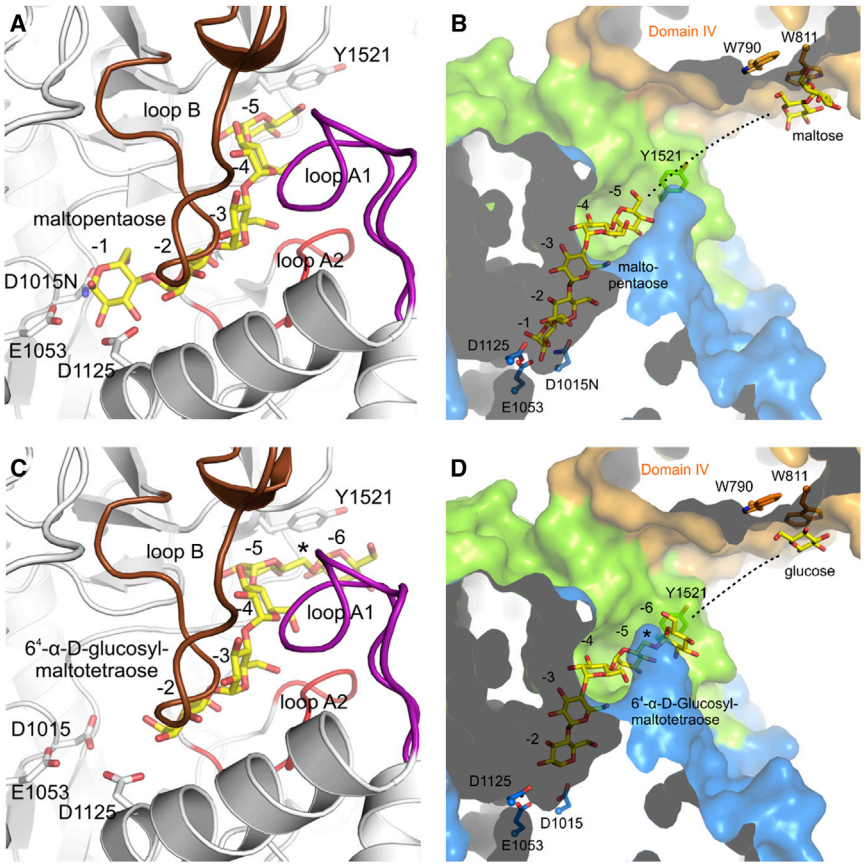

Figure 3. Binding of Oligosaccharides in the Tunnel at the Donor Side of GtfB-ΔNΔV

Binding of oligosaccharides: maltopentaose in subsites −1 to −5 of GtfB-ΔNΔV D1015N (A and C), and a mixed isomalto-/maltooligosaccharide transglycosylation product (6^4-α-D-glucosyl-maltotetraose) in subsites −2 to −6 of GtfB-ΔNΔV (B and D). The α-1,6-linkage at the non-reducing end of 6^4-α-D-glucosyl-maltotetraose is indicated (asterisk).

(A and B) The tunnel is covered by loops A1 (purple) and loop B (brown) at subsites −2 and −3. The catalytic residues are indicated as well as residue Y1521.

(C and D) Protein is represented as surface representation with domain colored as in Figure 1. The remote carbohydrate-binding site in domain IV (residues W790 and W811) at the extension of the donor sites as indicated by the dotted line has a maltose or glucose bound, respectively.

See also Figures S3 and S4.

Mechanism and Mode of Action of GtfB in Comparison with α-Amylase and Glucansucrase

The first step in the 4,6-α-GT reaction is donor substrate binding across the cleavage site. Modeling a maltooligosaccharide in GtfB-ΔNΔV by superposition with an α-amylase (see above) showed that the binding modes likely are very similar (Figure 5A), such that maltooligosaccharides can enter the tunnel and occupy multiple donor subsites (Figure 6). All our soaking experiments revealed oligosaccharides occupying multiple donor subsites, suggesting that the affinity for donor subsites is higher than for acceptor subsites. The presence of loops A1 and B, unique to 4,6-α-GTs, likely contributes to a higher affinity at donor subsites beyond −1 than in α-amylases by shielding these subsites from the solvent. Moreover, several residues from loop A2 that are different in α-amylases provide interactions to the bound maltooligosaccharides (Figure S3, related to Figure 3).

After binding, donor substrates are cleaved; incubation of GtfB-ΔN with a blocked substrate (Figure S5, related to Figure 6) shows that the enzyme can act not only exo- but also endolytically. The general acid/base (E1053) attacks the glycosidic bond between subsites −1 and +1, and the catalytic nucleophile (D1015) attacks the C1 of the glucosyl moiety in subsite −1, resulting in formation of a covalent intermediate with this residue. Given the high conservation of subsite −1, this covalent intermediate will have a similar conformation as in α-amylases and glucansucrases.

The subsequent step is either hydrolysis or transglycosylation. In the case of hydrolysis, an acceptor water molecule attacks the covalent intermediate at its C1 atom. Alternatively, if the acceptor substrate is a sugar moiety, transglycosylation takes place. Linkage type specificity is governed by the orientation of the incoming acceptor substrate, which in turn is determined by residues surrounding positive subsites. While GSs have different linkage specificities (α-1,2, α-1,3, α-1,4, or α-1,6) and α-amylases only display α-1,4 specificity, the 4,6-α-GTs prefer the formation of α-1,6 linkages in the second half reaction. Investigating acceptor binding in GtfB-ΔNΔV by modeling panose (a better acceptor substrate than maltotriose, see Bai et al., 2016b) showed that this trisaccharide is able to bind in a productive orientation in subsites +1 to +3 for the formation of an α-1,6 glycosidic linkage with the covalent intermediate (Figure 5B). At subsite +1, residues E1053 (motif III, the catalytic acid/base), N1019 (motif II), and L971 (domain B) seem critical for the orientation of the glucosyl unit. At subsites +2 and +3, residues (N1129 in motif IV and Y1079 in helix α4) may help orient the acceptor, while residue Y1055 (motif III) may provide a non-specific hydrophobic stacking platform at subsite +2, similar to the corresponding tryptophan residue in GSs. Some of these residues (N1129, Y1055, and Y1079) are specific to and conserved in 4,6-α-GTs (Figure 2B), and thus may contribute to the α-1,6-transglycosylation specificity.

Transglycosylation products are mixed isomalto-/maltooligosaccharides, which may diffuse out of the active site; however, the observation of a transglycosylation product bound at subsites −2 to −6 from soaking wild-type GtfB-ΔNΔV crystals with G6 (Figures 3C and 3D) shows that it is possible that after a single transglycosylation step the product can shift along the binding groove in the donor direction, in this case by five positions. Such a shift can, after formation of the α-1,6-linkage, position transglycosylation products such that the preference of subsites −1 and +1 for an α-1,4 linked maltosyl section is met, thus facilitating the next cleavage event. Indeed, mixed isomalto-/maltooligosaccharides such as those shown in Figure S6

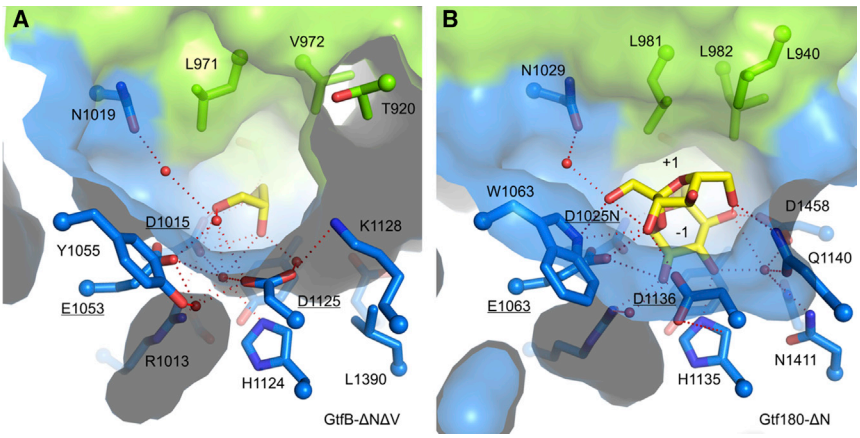

Figure 4. Active-Site Comparison of a 4,6-α-GT and a GS

(A and B) Comparison of *L. reuteri* 121 GtfB-ΔNΔV (this work; molecule A of the asymmetric unit is shown, A) with the *L. reuteri* 180 Gtf180-ΔN - sucrose complex (B) (Vujičić-Žagar et al., 2010). Blue represents domain A and green represents domain B. Catalytic residues are underlined. In Gtf180-ΔN, the fructosyl moiety in subsite +1 has hydrogen bond interactions (red dotted lines) with residues Q1140 and W1065 and, via a water-mediated hydrogen bond network, with residues N1411 and D1458. In GtfB-ΔNΔV, the corresponding residues are K1128, Y1055, and L1390, but the fourth residue is absent; moreover, the side chains of Y1055 and L1390 are unable to make hydrogen bonds. Finally, differences in residues of domain B cause the active-site pocket to be wider in GtfB-ΔNΔV. See also Figure S6.

(related to Figure 6) are processed by GtfB-ΔN, which is only possible if they occupy multiple donor subsites. This is in agreement with earlier conclusions that the enzyme becomes a better transglycosylase after the first transglycosylation products have been formed (Leemhuis et al., 2013b). Thus, first transglycosylation products can undergo a next reaction cycle (Figure 6, panel *II*); if they stay bound to the enzyme before doing so, this would represent a processive mode of action in 4,6-α-GTs. In any case, the reaction scheme proposed here explains all of the oligosaccharides observed upon incubation of GtfB with different maltooligosaccharides (Dobruchowska et al., 2012; Leemhuis et al., 2013b).

The soaking experiments also revealed three additional carbohydrate-binding sites remote from the active site. One site is near W790 and W811 in domain IV, and lies more or less in line with the donor tunnel at a distance of about two or three glucosyl units (16 Å) from subsite −6 (Figures 3B and 3D). Soaking of GtfB-ΔNΔV crystals with different maltooligosaccharides frequently showed electron density for bound carbohydrates at this site. Notably, the W790/W811 tryptophan pair is unique to and conserved in 4,6-α-GTs. The other remote sites are in domain A, near the β6-α7 and β7-α8 loops, and near helices α2 and α3. The bound saccharides make only a few interactions with the protein; the interacting residues are not conserved in 4,6-α-GTs.

Genomic and Phylogenetic Analysis

Querying the NCBI database with the *L. reuteri* 121 GtfB sequence yielded 47 putative 4,6-α-GTs (identity >50%), mostly in *Lactobacillus* strains. Genomic mapping of fully or partially

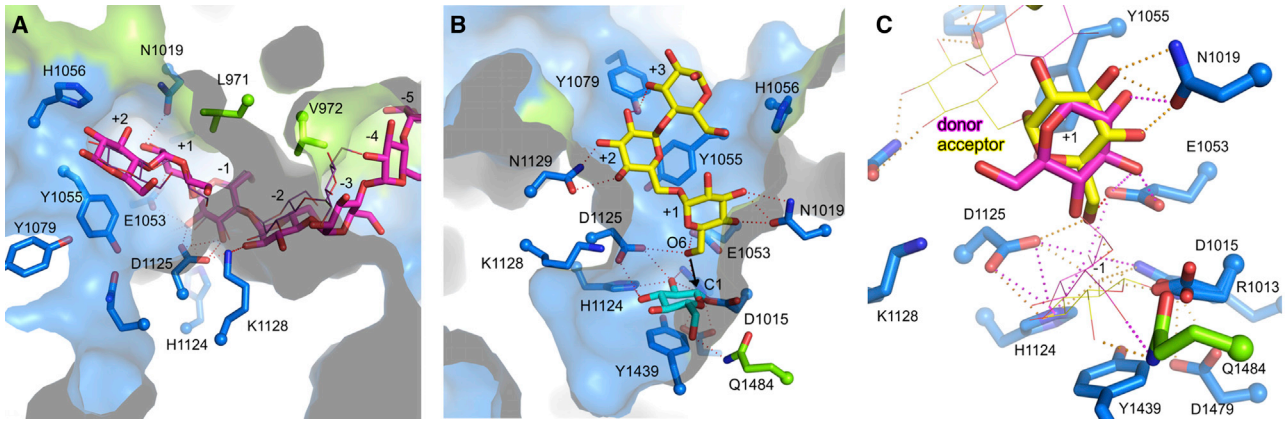

Figure 5. Donor and Acceptor Substrate Binding in GtfB-ΔNΔV

(A) Model for donor substrate binding in GtfB-ΔNΔV across the cleavage site: maltoheptaose (magenta carbon atoms) bound in subsites −5 to +2, based on the maltopentaose-bound crystal structure. The maltopentaose bound in subsites −3 to +2 of *B. subtilis* α-amylase (Fujimoto et al., 1998) is shown in a wire-frame representation with purple carbon atoms. Putative hydrogen bond interactions (dotted lines) with the modeled maltoheptaose in subsites −1, +1, and +2 are indicated; residue Y1055 may provide a hydrophobic stacking interactions at subsite +2. At the reducing end there is space for more sugar units.

(B) View (from a different angle) of the model for acceptor substrate binding; panose (yellow carbon atoms) is bound in subsites +1 to +3 of the covalent glucosyl-enzyme intermediate model of GtfB-ΔNΔV (cyan carbon atoms). In this orientation, the O6 atom of the non-reducing end glucosyl unit of panose can attack the C1 atom of the covalent intermediate to form an α-1,6 glycosidic linkage.

(C) Superposition of the models in (A) and (B), bound in a donor situation (magenta carbon atoms and hydrogen bonds) or acceptor situation (yellow carbon atoms, orange hydrogen bonds), highlighting the rotation and shift of the glucosyl unit in subsite +1 (stick representation).

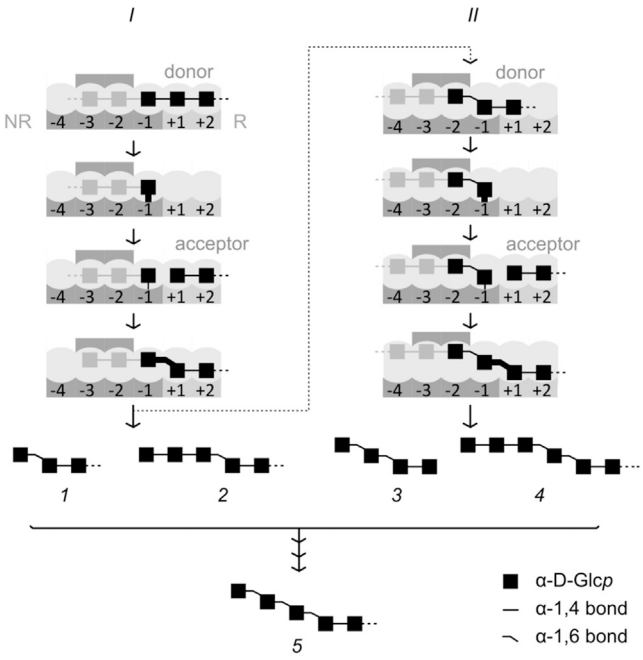

Figure 6. Proposed Reaction Pathways of 4,6-α-GTs

R, reducing end; NR, non-reducing end; four of the six donor subsites are indicated, of which subsites −2 and −3 are in the tunnel. Newly formed bonds are indicated with thicker lines. Binding of maltooligosaccharide donor substrates (panel *I*) involves a single subsite, or multiple ones (gray units) in the tunnel, yielding mixed isomalto-/maltooligosaccharide transglycosylation products of types *1* and *2*, respectively. Type *2* products can become donor substrates for a next cycle (panel *II*); whether they first diffuse out or stay bound to the enzyme and shift is currently unclear. The resulting transglycosylation products are of types *3* and *4*. Eventually, all products are mixed isomalto-/maltooligosaccharides with α-1,6 linked glucosyl units at their non-reducing end. See also Figures S5 and S6.

sequenced 4,6-α-GTs (Figure S7, related to Figure 7) revealed that in several *Lactobacillus* strains the 4,6-α-GT gene coexists with a GS gene.

The two gene products of such pairs show high length and sequence homology (see below) and are flanked by one or more transposase genes. This suggests that the 4,6-α-GT/GS pairs are the result of gene duplication events facilitated by transposases. A phylogenetic analysis of the catalytic cores (domains A and B) of GH70 and GH13 enzymes (Figure 7) revealed that the GSs and 4,6-α-GTs are more closely related to each other than to GH13 members. The GH70 enzymes likely have a common ancestor that is closely related to and likely evolved from maltooligosaccharide-processing α-amylases of GH13 subfamily 5; phylogenetically, they are much more distant from members of GH13 that are active on sucrose (e.g., subfamilies 4 and 18).

In Vivo Experiments

Growth of a fructansucrase-negative mutant of *L. reuteri* 121 (*L. reuteri* 35-5) on either sucrose or maltodextrins (containing 5% α-1,6 linkages and 95% α-1,4 linkages) on agar plates resulted in the formation of transparent colonies surrounded by a slimy halo (Figure 8A); in contrast, growth on glucose did not yield such halos. Previously, it has been shown that the EPS formed by *L. reuteri* 35-5 from sucrose is a reuteran containing both α-1,6 and α-1,4 linkages (van Leeuwen et al., 2008). Nuclear magnetic resonance (NMR) analysis (Figure 8B) showed that the polysaccharide present in the halos, derived from the maltodextrin-grown cultures, is also a reuteran-like EPS, with 61% α-1,6 linkages and 39% α-1,4 linkages. Size-exclusion chromatography (SEC) analysis of the polysaccharides isolated from the halos of plated cultures (Figure 8C) revealed that the synthesized reuteran-like EPS are approximately of the same size (35 MDa).

In-gel periodic acid-Schiff (PAS) staining of enzymes (Figure 8D) revealed that, when incubated with sucrose substrate, the constitutively expressed glucansucrase GtfA (199 kDa) is associated with reuteran synthesis, in agreement with earlier studies (van Geel-Schutten et al., 1999; Kralj et al., 2002). When *L. reuteri* 35-5 was supplied with maltodextrins, not GtfA but the 4,6-α-glucanotransferase GtfB was associated with reuteran synthesis. When incubated with a mixture of sucrose and maltodextrins, both GtfA and GtfB are associated with reuteran synthesis. Notably, *L. reuteri* 121 genomic data suggest that the only carbohydrate-acting enzymes larger than 150 kDa are GtfA and GtfB (Bai et al., 2016a).

DISCUSSION

The crystal structure of *L. reuteri* 121 GtfB-ΔNΔV shows that its active-site architecture is intermediate between GH13 α-amylases and GH70 glucansucrases, with an α-amylase-like binding groove partly covered by long loops forming a tunnel. Phylogenetic and genomic analyses suggest that 4,6-α-GTs and GSs evolved from a common ancestor close to maltooligosaccharide-processing α-amylases of subfamily GH13_5 (Figure 7). Importantly, the α-amylase binding groove is retained in 4,6-α-GTs but the reaction specificity has evolved toward a 6-α-specific transglycosylation activity. A similar evolutionary path has been proposed for the recently identified GtfC subfamily (Gangoiti et al., 2015). Thus, we propose that the 4,6-α-GT functionality evolved first; further evolution toward GS specificity allowed lactobacilli to synthesize α-glucans from sucrose. The GtfB-ΔNΔV crystal structure supports this hypothesis and details the accompanying structural changes (Figures 1B and 9).

The likely structural determinants of the change in reaction specificity from hydrolysis (in α-amylases) to transglycosylation (in 4,6-α-GTs) are the long loops A1 and B that create a tunnel in GtfB-ΔNΔV (and likely in other 4,6-α-GTs). Although GtfB-ΔNΔV can bind maltooligosaccharide donor substrates in a similar way as α-amylases, the observation that all soaking experiments resulted in occupied tunnel subsites (−2, −3) suggests that these loops enhance oligosaccharide binding at the donor side. This idea is further supported by the impaired transglycosylation and polymerization activity of a mutant (T920W) with a blocked tunnel (Figures S1 and S2, related to Figure 6). The presence of the tunnel also explains why the enzyme only processes linear segments of starch and prefers high-amylose starches as substrate (Leemhuis et al., 2014; Bai et al., 2015, 2016a). Finally, it suggests that 4,6-α-GTs have endolytic activity, whereby multiple glucosyl units are transferred (Figure 6). The resulting mixed isomalto-/maltooligosaccharides can become donor substrates in a next reaction cycle, as shown by the results of incubating GtfB-ΔN with a blocked

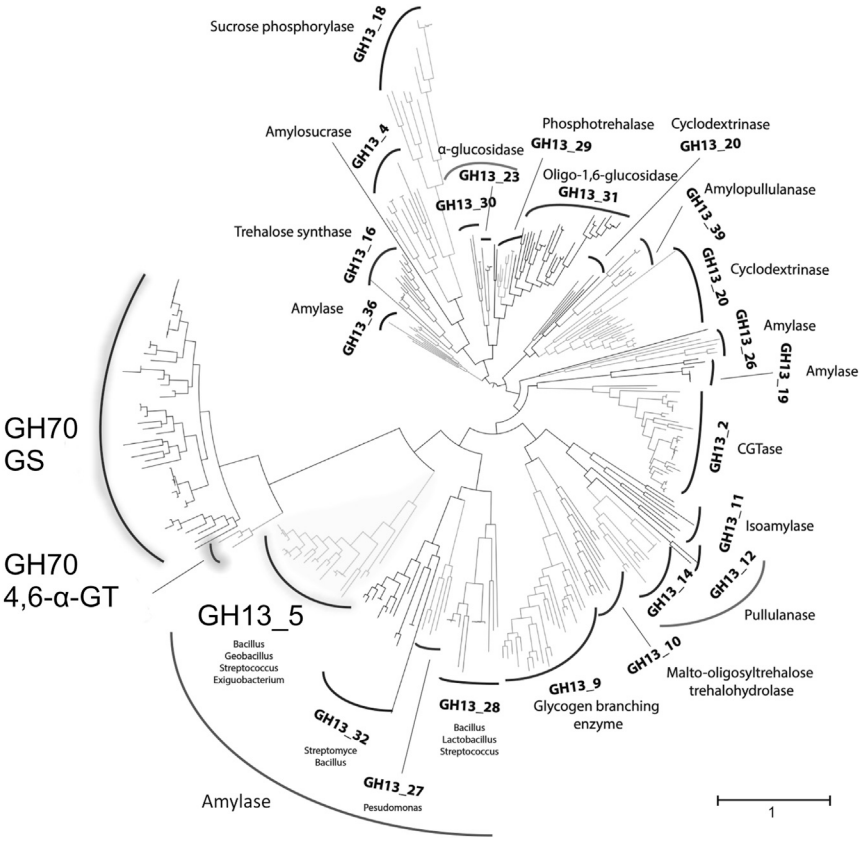

Figure 7. Phylogenetic Tree of Family GH13 and GH70

The bacterial protein sequences were all characterized based on CAZY database (http://www.cazy.org; Lombard et al., 2014). Domains A and B of GH70 members were extracted and rearranged according to the (non-circularly permuted) GH13 domain arrangement. The GH70 4,6-α-GTs and GSs are closely related to α-amylases from GH13 subfamily 5 (GH13_5), which are found in Gram-positive bacterial species such as *Streptococcus*, *Bacillus*, and *Exigobacterium*. Also, GH70 enzymes are mainly found in Gram-positive bacteria, supporting our hypothesis about the evolutionary events leading to their different specificities. On the other hand, GH70 4,6-α-GTs and GSs are far from sucrose-acting GH13 enzymes from subfamilies 4 and 18. See also Figure S7.

substrate (Figure S5, related to Figure 6) or with mixed isomalto-/maltooligosaccharides (Figure S6, related to Figure 6). This explains the observed product spectrum (Dobruchowska et al., 2012). The tunnel-forming loops covering donor subsites −2 and −3 may confer processivity to the enzyme (Breyer and Matthews, 2001; van Pouderoyen et al., 2003) by keeping isomalto-/maltooligosaccharides bound between reaction cycles and in this way increase the efficiency of polymer synthesis by 4,6-α-GTs. How the structure of the GtfB-ΔNΔV active site limits hydrolytic activity is currently unknown, but earlier in vitro studies have shown that the enzyme efficiently transglycosylates its substrates and synthesizes polymers with a degree of polymerization up to 35 (Leemhuis et al., 2014). In this regard, it will also be interesting to see the loop architecture in GtfC-type 4,6-α-GTs; attempts to obtain structural information of these enzymes are in progress in our laboratories. On the other hand, our models for donor/acceptor binding and mutant studies suggest that in addition to the loops, single residues (e.g., Y1055, K1128, and N1019) also contribute to the ability of the enzyme to synthesize polymers and to efficiently α-1,6-transglycosylate its substrates, for example by facilitating the binding of glucosyl units in an extra orientation (Figure 5). This further supports the proposed evolution of 4,6-α-GTs from hydrolytic α-amylases. Further evolution of 4,6-α-GTs to GSs involved a change in preferred donor substrate (from maltooligosaccharides to sucrose). Since subsite −1 remained virtually unchanged, we propose that structural changes in subsite +1 involved residues Y1055/W1065, K1128/Q1140 (GtfB/GTF180 numbering), and small hydrophobic residues from domain B; these changes affect hydrogen-bonding capabilities and binding space for donor substrates, shifting binding preference from an α-1,4-linked glucosyl to an α-1,2-linked fructosyl unit. In addition, elongation and repositioning of loop A2, blocking donor subsites beyond −1 (Figures 1B and 9), limits transglycosylation in GSs to single glucosyl units. Concurrently, loops A1 and B may have become shorter because they were no longer needed to cover donor subsites beyond −1 (Figure 9).

Even though the 4,6-α-GT function can be regarded as an evolutionary intermediate, the presence of either a single 4,6-α-GT gene, a single GS gene, or 4,6-α-GT/GS gene pairs (Figure S7, related to Figure 7), indicates that evolution did not proceed similarly in all *Lactobacillus* species. First, the occurrence of 4,6-α-GT/GS gene pairs in several species can be explained by a neofunctionalization model involving duplication of the ancestral gene (He and Zhang, 2005; Roth et al., 2007). Indeed, all *Lactobacillus* GH70 gene pairs have high internal homology and are flanked by transposase genes that likely facilitated the duplication. After duplication, one gene would retain its 4,6-α-GT specificity and the other one would acquire GS specificity under the positive constraint of sucrose presence. Second, the presence of single 4,6-α-GT or GS genes in other species can be explained by horizontal gene transfer and evolution of single genes, similar to what has been proposed for GSs of oral *Streptococcus* and *Leuconostoc* species (Fujiwara et al., 1998; Simpson et al., 1995; Passerini et al., 2015; Hoshino et al., 2012).

The proposed evolution of carbohydrate-acting enzymes in oral bacteria involves remarkable changes in product specificity and substrate specificity. The underlying evolutionary mechanisms are proposed to be driven by constraints such as the availability of different substrates in the organism's habitat or the capability to survive (Qian and Zhang, 2014). Regarding the evolution of α-amylase/4,6-α-GT/GS enzymes of oral

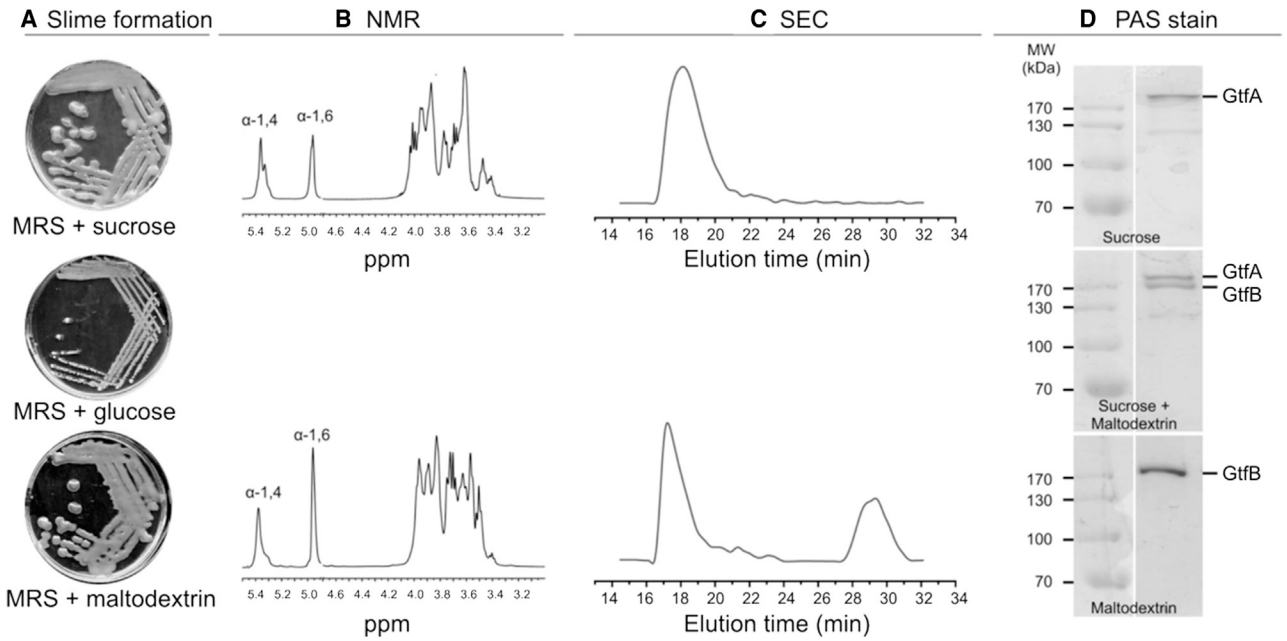

Figure 8. In Vivo EPS Formation by *L. reuteri* 35-5

(A) Growth of *L. reuteri* 35-5 on MRS agar supplemented with different carbon sources, forming slimy (sucrose, maltodextrins) or non-slimy colonies (glucose).

(B) One-dimensional ^{1}H NMR analysis of the EPS extracted from slimy colonies on agar plates with sucrose and maltodextrins showed that their composition is comparable with respect to glycosidic linkage type (α-1,4 and α-1,6).

(C) SEC analysis of the EPS extracted from slimy colonies on agar plates revealed that the extracellular polysaccharides derived from either sucrose or maltodextrins are similar in size distribution (~30 MDa). The peak at ≈18 min in both chromatograms represents the synthesized high molecular mass polysaccharides (≈35 MDa); the peak at ≈29 min in the chromatogram of the EPS isolated from the MRS + maltodextrin plate represents large molecular mass (≈5 kDa) maltodextrin substrates simultaneously precipitated by ethanol. Therefore, both NMR and SEC results suggest that providing *L. reuteri* 35-5 with either sucrose or maltodextrins as a carbon source results in formation of EPS with a similar linkage and size distribution.

(D) PAS-stained SDS-PAGE gel of whole-cell proteins of *L. reuteri* 35-5 grown in the presence of either sucrose, sucrose + maltodextrin, or maltodextrin, revealing the association of bands corresponding to the molecular weights of either the glucansucrase GtfA (199 kDa) or the 4,6-α-glucanotransferase GtfB (179 kDa) with the production of sucrose-derived EPS or of maltodextrin-derived EPS, respectively. The minor band at ~120 kDa may represent an N-terminally truncated form (GtfA-ΔN) due to the protein extraction process; however, as reported previously, GtfA-ΔN synthesizes a reuteran very similar in size distribution and linkage type to that produced by the full-length enzyme (van Geel-Schutten et al., 1999; Kralj et al., 2002). Adapted from Bai et al. (2016b).

bacteria, the most likely driving factors are changes in the carbohydrate composition of the human diet over time. Interestingly, the use of refined carbohydrates (including sucrose) for food production correlates with a sharp increase in the incidence of caries in industrialized countries (Touger-Decker and van Loveren, 2003). The importance of biofilms for cariogenesis and the contribution of GS-synthesized α-glucans to biofilm formation in vivo thus likely links the evolution of GS enzymes with an increase in dietary sucrose. However, more moderate and temporary increases in the prevalence of caries have occurred long before industrialization, when the human diet consisted of foods containing hardly any sucrose but was rich in starch (Yudkin, 1967; Ganzle and Follador, 2012). We recently showed that several *L. reuteri* strains utilize starch-derived maltodextrins to synthesize α-glucans in vivo, and that the responsible enzyme is a 4,6-α-GT such as GtfB (Bai et al., 2016a) (Figure 8). We propose that the 4,6-α-GT enzymes evolved when during relatively affluent times staple foods were subjected to cooking, a process that makes the starch components more susceptible to amylolytic breakdown (Lingstrom et al., 2000), and that this promoted the evolution of enzymes able to use the resulting oligosaccharide fragments, from already existing starch-processing α-amylases, as substrates (Figure 7). The 4,6-α-GT activity enabled the bacteria to synthesize extracellular polymers with α-1,6-linkages resistant to oral α-amylases, and to form biofilms that promoted cariogenesis. We propose that further evolution toward GS activity occurred under the positive selection of a widespread consumption of sucrose, facilitating α-glucan synthesis from a simpler substrate and, as suggested by kinetic data, also enhancing the catalytic efficiency (Kralj et al., 2005; Newton et al., 2015). Thus, as shown by our in vivo experiments (Figure 8), *L. reuteri* strains with 4,6-α-GT/GS gene pairs have an additional advantage of being able to synthesize α-glucans from both starch-derived maltooligosaccharides and sucrose.

Thus, the crystal structure of GtfB-ΔNΔV clearly suggests that the GH70 4,6-α-glucanotransferase subfamily is intermediate in the evolution of glucansucrases from α-amylases, and phylogenetic and genomic analysis further supports this finding. The unique active-site architecture of GtfB-ΔNΔV reveals how, evolving from starch-processing α-amylases, the elongation and repositioning of three loops facilitates the transglycosylation of starch-derived maltooligosaccharides by 4,6-α-GTs. Evolution toward the different substrate specificity observed in GSs likely

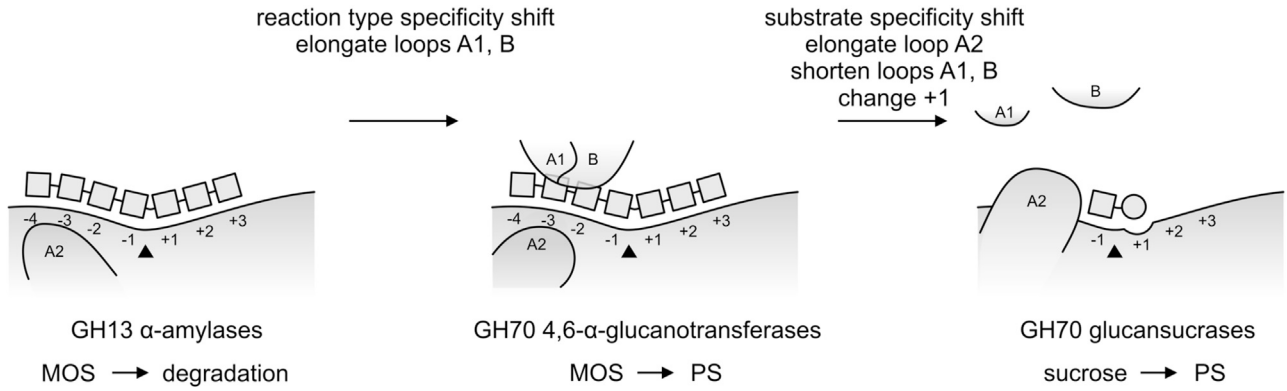

Figure 9. Evolutionary Relationships between α-Amylases, 4,6-α-Glucanotransferases, and Glucansucrases

The catalytic site for cleavage and transglycosylation (traingles) is between subsites −1 and +1. The α-amylases that process maltooligosaccharides (MOS; squares represent glucose units) have an open binding groove with multiple donor and acceptor subsites; they lack loops A1 and B, and are unable to synthesize polysaccharides (PS). The 4,6-α-glucanotransferases acquired this capability via elongation of loops B and A1 forming a tunnel at the donor half of the groove, allowing them to capture better the intermediate for subsequent transglycosylation and thus shift their product specificity toward glucan polysaccharides. Subsequently, a shift in substrate specificity was obtained by elongation of loop A2, which blocks donor subsites beyond −1, and by changes in subsite +1; loops A1 and B became shorter and in this way, glucansucrases acquired the capability to utilize sucrose (the circle represents a fructose unit) for the synthesis of glucan polysaccharides. The more open architecture of the GS active site may explain their ability to form branched α-glucans whereas the 4,6-α-GTs, due to the tunnel, only synthesize linear ones.

was accompanied by further changes in the same loops as well as in acceptor subsite +1. Importantly, in vivo not only GSs but also 4,6-α-GTs contribute to α-glucan synthesis in *L. reuteri*. This suggests that biofilm formation by oral bacteria, and the prevalence of dental caries, is related not only to the intake of dietary sucrose but also to that of starch and starch-derived oligosaccharides. We propose that dietary changes involving starch and sucrose intake were important factors during the evolution of 4,6-α-GTs and (later) GSs from α-amylases, allowing the bacteria to produce extracellular polymers from different substrates.

EXPERIMENTAL PROCEDURES

Details of experimental procedures and program references can be found in Supplemental Experimental Procedures.

Cloning, Truncation and Site-Directed Mutagenesis, Expression, Purification, and Characterization

The truncation strategy, cloning, and mutagenesis of gtfB-ΔN and gtfB-ΔNΔV are described in Supplemental Experimental Procedures. Expression and purification of GtfB-ΔN was performed as described by Bai et al. (2015); expression and purification of GtfB-ΔNΔV and its mutants followed a similar procedure with a modification. Details of enzyme characterization are given in Supplemental Experimental Procedures.

Crystallization, Soaking Experiments, and Data Collection

GtfB-ΔNΔV was crystallized by the hanging-drop vapor diffusion method and a microseeding protocol. For soaking experiments, the stabilizing solution was supplemented with 50 mM maltohexaose (10 min, wild-type GtfB-ΔNΔV crystals) or 100 mM maltopentaose (8 min, GtfB-ΔNΔV D1015N crystals). Datasets were collected at the European Synchrotron Radiation Facility at beamlines ID23-2 and ID23-1, respectively, at 100 K; details and processing statistics are given in Table 1.

Structure Determination

The structure of GtfB-ΔNΔV was determined by molecular replacement using domains A, B, C, and IV of the crystal structure of *L. reuteri* 180 GTF180-ΔN (PDB: 3KLK; Vujičić-Žagar et al., 2010) as a search model (sequence identity = 39.6%), and refined by alternating cycles of restrained refinement with REFMAC5 (Murshudov et al., 1997) and model building with Coot (Emsley et al., 2010). The asymmetric unit contained two molecules of GtfB-ΔNΔV (Figure 1A). Coordinates and structure factors have been deposited at the PDB (PDB: 5JBD, wild-type native; 5JBE, wild-type maltohexaose soak; 5JBF, D1015N maltopentaose soak).

Modeling and Docking

We modeled donor substrate binding and acceptor substrate binding (panose) to a covalent glucosyl-enzyme intermediate in GtfB-ΔNΔV by using related structures of α-amylases, a cyclodextrin glycosyltransferase, and glucansucrases. The results are shown in Figures 5A and 5B, respectively.

Genomic Mapping and Phylogenetic Analysis

The location of the genes encoding 4,6-α-GT and GS proteins from *L. reuteri* strains were obtained based on the graphics data in the NCBI database. We analyzed the phylogenetic relation between all bacterial GH13 and GH70 enzymes; for the latter, domains A and B were rearranged to "correct" for the circular permutation of the $(\beta/\alpha)_8$ barrel $(B_NA_N\cdots A_CB_C \rightarrow A_CB_CB_NA_N$; the subscript denotes either the N- or C-terminal segment). The rearranged GH70 sequences were then included in the alignment of all characterized GH13 members classified into subfamilies. Homologs of full-length GtfB were searched using Protein-BLAST in the NCBI (http://www.ncbi.nlm.nih.gov) and UniProtKB (http://www.uniprot.org) databases.

In Vivo Experiments

Growth conditions of plate-grown *L. reuteri* are described in Supplemental Experimental Procedures. Whole-cell proteins produced by *L. reuteri* were extracted and analyzed by SDS-PAGE; the EPS-producing enzymes herein were identified using an activity staining method (PAS). The EPS produced in the cultures were extracted and analyzed by enzymatic hydrolysis, monosaccharide analysis using high-performance anion-exchange chromatography, SEC, NMR spectroscopy, and thin-layer chromatography.

SUPPLEMENTAL INFORMATION

Supplemental Information includes Supplemental Experimental Procedures, seven figures, and two tables and can be found with this article online at http://dx.doi.org/10.1016/j.str.2016.11.023.

AUTHOR CONTRIBUTIONS

Conceptualization, B.W.D., L.D., and T.P.; Methodology, Y.B. and T.P.; Investigation, Y.B., J.G., and T.P.; Writing – Original Draft, Y.B., J.G., and T.P.; Writing – Review & Editing, Y.B. and T.P.; Funding Acquisition, Y.B. and L.D.; Supervision, B.W.D. and L.D.

ACKNOWLEDGMENTS

Y.B. was financially supported by the China Scholarship Council, the University of Groningen. Y.B. and J.G. were financially supported by the TKI Agri & Food Program as coordinated by the Carbohydrate Competence Center (CCC-ABC; www.cccresearch.nl). Staff of the European Synchrotron Radiation Facility (Grenoble, France) beamlines are acknowledged for assistance with diffraction data collection.

Received: August 25, 2016
Revised: November 3, 2016
Accepted: November 28, 2016
Published: January 5, 2017

REFERENCES

Bai, Y., van der Kaaij, R.M., Leemhuis, H., Pijning, T., van Leeuwen, S.S., Jin, Z., and Dijkhuizen, L. (2015). Biochemical characterization of the *Lactobacillus reuteri* glycoside hydrolase family 70 GTFB type of 4,6-α-glucanotransferase enzymes that synthesize soluble dietary starch fibers. Appl. Environ. Microbiol. *81*, 7223–7232.

Bai, Y., Böger, M., van der Kaaij, R.M., Woortman, A.J., Pijning, T., van Leeuwen, S.S., van Bueren, A.L., and Dijkhuizen, L. (2016a). *Lactobacillus reuteri* strains convert starch and maltodextrins into homoexopolysaccharides using an extracellular and cell-associated 4,6-α-glucanotransferase. J. Agric. Food Chem. *64*, 2941–2952.

Bai, Y., Dobruchowska, J.M., Van der Kaaij, R.M., Gerwig, G.J., and Dijkhuizen, L. (2016b). Structural basis for the roles of starch and sucrose in homo-exopolysaccharide formation by *Lactobacillus reuteri* 35-5. Carbohydr. Polym. *151*, 29–39.

Breyer, W.A., and Matthews, B.W. (2001). Protein Sci. *10*, 1699–1711.

Brison, Y., Pijning, T., Malbert, Y., Fabre, É., Mourey, L., Morel, S., Potocki-Véronèse, G., Monsan, P., Tranier, S., Remaud-Siméon, M., and Dijkstra, B.W. (2012). Functional and structural characterization of α-(1→2) branching sucrase derived from DSR-E glucansucrase. J. Biol. Chem. *287*, 7915–7924.

Carlsson, J., Grahnen, H., and Jonsson, G. (1975). Lactobacilli and streptococci in the mouth of children. Caries Res. *9*, 333–339.

Davies, G.J., Wilson, K.S., and Henrissat, B. (1997). Nomenclature for sugar-binding subsites in glycosyl hydrolases. Biochem. J. *321*, 557–559.

Dobruchowska, J.M., Gerwig, G.J., Kralj, S., Grijpstra, P., Leemhuis, H., Dijkhuizen, L., and Kamerling, J.P. (2012). Structural characterization of linear isomalto-/malto-oligomer products synthesized by the novel GTFB 4,6-α-glucanotransferase enzyme from *Lactobacillus reuteri* 121. Glycobiology *22*, 517–528.

Emsley, P., Lohkamp, B., Scott, W.G., and Cowtan, K. (2010). Features and development of Coot. Acta Crystallogr. D Biol. Crystallogr. *66*, 486–501.

Flemming, H.C., and Wingender, J. (2010). The biofilm matrix. Nat. Rev. Microbiol. *8*, 623–633.

Fujiwara, T., Terao, Y., Hoshino, T., Kawabata, S., Ooshima, T., Sobue, S., Kimura, S., and Hamada, S. (1998). Molecular analyses of glucosyltransferase genes among strains of *Streptococcus mutans*. FEMS Microbiol. Lett. *161*, 331–336.

Fujimoto, Z., Takase, K., Doui, N., Momma, M., Matsumoto, T., and Mizuno, H. (1998). Crystal structure of a catalytic-site mutant alpha-amylase from *Bacillus subtilis* complexed with maltopentaose. J. Mol. Biol. *277*, 393–407.

Gangoiti, J., Pijning, T., and Dijkhuizen, L. (2015). The *Exiguobacterium sibiricum* 255-15 GtfC enzyme represents a novel glycoside hydrolase 70 subfamily of 4,6-α-glucanotransferase enzymes. Appl. Environ. Microbiol. *82*, 756–766.

Ganzle, M.G., and Follador, R. (2012). Metabolism of oligosaccharides and starch in lactobacilli: a review. Front. Microbiol. *3*, 340.

He, X., and Zhang, J. (2005). Rapid subfunctionalization accompanied by prolonged and substantial neofunctionalization in duplicate gene evolution. Genetics *169*, 1157–1164.

Hoshino, T., Fujiwara, T., and Kawabata, S. (2012). Evolution of cariogenic character in *Streptococcus mutans*: horizontal transmission of glycosyl hydrolase family 70 genes. Sci. Rep. *2*, 518.

Ito, K., Ito, S., Shimamura, T., Weyand, S., Kawarasaki, Y., Misaka, T., Abe, K., Kobayashi, T., Cameron, A.D., and Iwata, S. (2011). Crystal structure of glucansucrase from the dental caries pathogen *Streptococcus mutans*. J. Mol. Biol. *408*, 177–186.

Koo, H., Xiao, J., Klein, M.I., and Jeon, J.G. (2010). Exopolysaccharides produced by *Streptococcus mutans* glucosyltransferases modulate the establishment of microcolonies within multispecies biofilms. J. Bacteriol. *192*, 3024–3032.

Koo, H., Falsetta, M.L., and Klein, M.I. (2013). The exopolysaccharide matrix: a virulence determinant of cariogenic biofilm. J. Dent. Res. *92*, 1065–1073.

Kralj, S., van Geel-Schutten, G.H., Rahaoui, H., Leer, R.J., Faber, E.J., van der Maarel, M.J., and Dijkhuizen, L. (2002). Molecular characterization of a novel glucosyltransferase from *Lactobacillus reuteri* strain 121 synthesizing a unique, highly branched glucan with α-(1→4) and α-(1→6) glucosidic bonds. Appl. Environ. Microbiol. *68*, 4283–4291.

Kralj, S., van Geel-Schutten, I.G., Faber, E.J., van der Maarel, M.J., and Dijkhuizen, L. (2005). Rational transformation of *Lactobacillus reuteri* 121 reuteransucrase into a dextransucrase. Biochemistry *44*, 9206–9216.

Kralj, S., Grijpstra, P., van Leeuwen, S.S., Leemhuis, H., Dobruchowska, J.M., van der Kaaij, R.M., Malik, A., Oetari, A., Kamerling, J.P., and Dijkhuizen, L. (2011). 4,6-α-glucanotransferase, a novel enzyme that structurally and functionally provides an evolutionary link between glycoside hydrolase enzyme families 13 and 70. Appl. Environ. Microbiol. *77*, 8154–8163.

Leemhuis, H., Pijning, T., Dobruchowska, J.M., van Leeuwen, S.S., Kralj, S., Dijkstra, B.W., and Dijkhuizen, L. (2013a). Glucansucrases: three-dimensional structures, reactions, mechanism, alpha-glucan analysis and their implications in biotechnology and food applications. J. Biotechnol. *163*, 250–272.

Leemhuis, H., Dijkman, W.P., Dobruchowska, J.M., Pijning, T., Grijpstra, P., Kralj, S., Kamerling, J.P., and Dijkhuizen, L. (2013b). 4,6-α-Glucanotransferase activity occurs more widespread in *Lactobacillus* strains and constitutes a separate GH70 subfamily. Appl. Microbiol. Biotechnol. *97*, 181–193.

Leemhuis, H., Dobruchowska, J.M., Ebbelaar, M., Faber, F., Buwalda, P.L., van der Maarel, M.J., Kamerling, J.P., and Dijkhuizen, L. (2014). Isomalto/malto-polysaccharide, a novel soluble dietary fiber made via enzymatic conversion of starch. J. Agric. Food Chem. *62*, 12034–12044.

Lingstrom, P., van Houte, J., and Kashket, S. (2000). Food starches and dental caries. Crit. Rev. Oral Biol. Med. *11*, 366–380.

Lombard, V., Golaconda Ramulu, H., Drula, E., Coutinho, P.M., and Henrissat, B. (2014). The carbohydrate-active enzymes database (CAZy) in 2013. Nucleic Acids Res. *42*, D490–D495.

Machius, M., Declerck, N., Huber, R., and Wiegand, G. (1998). Activation of *Bacillus licheniformis* α-amylase through a disorder → order transition of the substrate-binding site mediated by a calcium-sodium-calcium metal triad. Structure *6*, 281–292.

Murshudov, G.N., Vagin, A.A., and Dodson, E.J. (1997). Refinement of macromolecular structures by the maximum-likelihood method. Acta Crystallogr. D Biol. Crystallogr. *53*, 240–255.

Newton, M.S., Arcus, V.L., and Patrick, W.M. (2015). Rapid bursts and slow declines: on the possible evolutionary trajectories of enzymes. J. R. Soc. Interf. *12*, pii: 20150036.

Paes Leme, A.F., Koo, H., Bellato, C.M., Bedi, G., and Cury, J.A. (2006). The role of sucrose in cariogenic dental biofilm formation—new insight. J. Dent. Res. *85*, 878–887.

Passerini, D., Vuillemin, M., Ufarté, L., Morel, S., Loux, V., Fontagné-Faucher, C., Monsan, P., Remaud-Siméon, M., and Moulis, C. (2015). Inventory of the

GH70 enzymes encoded by *Leuconostoc citreum* NRRL B-1299-identification of three novel α-transglucosylases. FEBS J. *282*, 2115–2130.

Pijning, T., Vujičić-Žagar, A., Kralj, S., Dijkhuizen, L., and Dijkstra, B.W. (2012). Structure of the α-1,6/α-1,4-specific glucansucrase GTFA from *Lactobacillus reuteri* 121. Acta Crystallogr. Sect. F Struct. Biol. Cryst. Commun. *68*, 1448–1454.

Qian, W., and Zhang, J. (2014). Genomic evidence for adaptation by gene duplication. Genome Res. *24*, 1356–1362.

Robert, X., and Gouet, P. (2014). Deciphering key features in protein structures with the new ENDscript server. Nucleic Acids Res. *42*, W320–W324.

Roth, C., Rastogi, S., Arvestad, L., Dittmar, K., Light, S., Ekman, D., and Liberles, D.A. (2007). Evolution after gene duplication: models, mechanisms, sequences, systems, and organisms. J. Exp. Zool. B Mol. Dev. Evol. *308*, 58–73.

Simpson, C.L., Giffard, P.M., and Jacques, N.A. (1995). *Streptococcus salivarius* ATCC 25975 possesses at least two genes coding for primer-independent glucosyltransferases. Infect. Immun. *63*, 609–621.

Touger-Decker, R., and van Loveren, C. (2003). Sugars and dental caries. Am. J. Clin. Nutr. *78*, 881S–892S.

Uitdehaag, J.C.M., Mosi, R., Kalk, K.H., van der Veen, B.A., Dijkhuizen, L., Withers, S.G., and Dijkstra, B.W. (1999). X-ray structures along the reaction pathway of cyclodextrin glycosyltransferase elucidate catalysis in the α-amylase family. Nat. Struct. Biol. *6*, 432–436.

van Geel-Schutten, G.H., Faber, E.J., Smit, E., Bonting, K., Smith, M.R., Ten Brink, B., Kamerling, J.P., Vliegenthart, J.F., and Dijkhuizen, L. (1999). Biochemical and structural characterization of the glucan and fructan exopolysaccharides synthesized by the *Lactobacillus reuteri* wild-type strain and by mutant strains. Appl. Environ. Microbiol. *65*, 3008–3014.

van Leeuwen, S.S., Kralj, S., van Geel-Schutten, I.H., Gerwig, G.J., Dijkhuizen, L., and Kamerling, J.P. (2008). Structural analysis of the α-D-glucan (EPS180) produced by the *Lactobacillus reuteri* strain 180 glucansucrase GTF180 enzyme. Carbohydr. Res. *343*, 1237–1250.

van Pouderoyen, G., Snijder, H.J., Benen, J.A., and Dijkstra, B.W. (2003). Structural insights into the processivity of endopolygalacturonase I from *Aspergillus niger*. FEBS Lett. *554*, 462–466.

Vujičić-Žagar, A., Pijning, T., Kralj, S., López, C.A., Eeuwema, W., Dijkhuizen, L., and Dijkstra, B.W. (2010). Crystal structure of a 117 kDa glucansucrase fragment provides insight into evolution and product specificity of GH70 enzymes. Proc. Natl. Acad. Sci. USA *107*, 21406–21411.

Xiao, J., Klein, M.I., Falsetta, M.L., Lu, B., Delahunty, C.M., III, Yates, J.R., Heydorn, A., and Koo, H. (2012). The exopolysaccharide matrix modulates the interaction between 3D architecture and virulence of a mixed-species oral biofilm. PLoS Pathog. *8*, e1002623.

Yudkin, J. (1967). Evolutionary and historical changes in dietary carbohydrates. Am. J. Clin. Nutr. *20*, 108–115.